Geomech. Geophys. Geo-energ. Geo-resour. (2024) 10:82
https://doi.org/10.1007/s40948-024-00805-6

ORIGINAL ARTICLE

Predicting the compressive strength of tight sandstone based on the low field NMR and pseudo-triaxial compression measurements

Xinmin Ge · Renxia Zhang · Jianyu Liu · Yiren Fan · Michael Myers · Lori Hathon

Received: 13 June 2022 / Accepted: 10 January 2024

Abstract The compressive strength is very important for petroleum and other engineering studies. However, the effect of pore size and fluid distribution on the rock's strength is not fully understood. We developed comprehensive research to study the controlling factors of the compressive strength based on low field nuclear magnetic resonance (NMR) measurements and pseudo-triaxial compression test for tight sandstones. The relationship between the compressive strength and the NMR obtained parameters are investigated completely, aiming for a better estimation of the compressive strength using the NMR data. The result shows that the rock's strength is strongly controlled by the pore size distribution and the fluid existing state. Generally, the compressive strength is negatively correlated with the average transversal relaxation time, the movable water saturation, and the porosity, but positively correlated with the irreducible water saturation. The result reveals that the rock with larger pore radius and higher percentage of movable fluid is easier to reach the failure state. Further, the precision of the empirical model by multiple regression of the geometric mean of the relaxation time and the porosity is greatly improved compared with the model established by the brittle minerals, which is potentially to be use for geophysical prospecting when the NMR logging data is available.

Highlights

1. The first time to use NMR to characterize the compressive strength.
2. Pore size control on the rock mechanical property is investigated.
3. Empirical equation is established to predict the compressive strength.

Keywords Compressive strength · Low field NMR measurement · Pseudo-triaxial compression test · Pore size · Fluid distribution · Tight sandstone

X. Ge (✉) · R. Zhang · Y. Fan
State Key Laboratory of Deep Oil and Gas, China University of Petroleum (East China), Qingdao 266580, China
e-mail: gexinmin2002@163.com

X. Ge · Y. Fan
Laboratory for Marine Mineral Resources, Qingdao Marine Science and Technology Center, Qingdao 266071, China

J. Liu
Northwest Branch, Research Institute of Petroleum Exploration and Development, PetroChina, Lanzhou 730000, China

M. Myers · L. Hathon
Petroleum Engineering Department, University of Houston, Houston 77204-0945, USA

Published online: 03 May 2024

1 Introduction

The compressive strength is defined as the resistance to failure under the action of compressive forces. It is an essential geomechanical parameter in many areas such as the exploration and development of minerals and fossil fuels, the evaluation of engineering disasters, the geotechnical investigation, as well as the civil infrastructures such as urban underground spaces, nuclear facilities, tunnels, high-rise buildings, and underground gas storage sites (Escartín et al. 2008; Yagiz 2009; Huang et al. 2012; Gullu and Hazirbaba 2010; Haimson 2011; Kapang et al. 2013; Rabah et al. 2014; Rohmer et al. 2016; Wang et al. 2020). Although the laboratory uniaxial or triaxial point load measurements can provide reliable compression strength data (Tsiambaos and Sabatakakis 2004), are time consuming and expensive (Negara et al. 2017). Therefore, it is imperative to finding an economic and convenient method to predict the compressive strength at the in-situ condition. The prediction is difficult since they are too many influential factors to be considered due to the fact that the rock is basically a poroelastic material, including mineralogical compositions, diagenetic process, bedding inclination, sedimentary environments, and pore fluids (Meng et al. 2006; Forquin et al. 2010; Zhao et al. 2012; Maleki and Bayat 2012; Pan et al. 2013; Luo et al. 2014; Zhong et al. 2014; Lisabeth and Zhu 2015; Ündül 2016; Dessouki et al. 2016; Peng et al. 2017; Fakir et al. 2017; Lou et al. 2018; Tang 2018; Yin and Yang 2018; Wang et al. 2019; Gharechelou et al. 2020). Pseudo-triaxial compression test is an experimental method that simulates the axisymmetric stress state by applying radial and circumferential stresses to replicate the stress conditions of underground materials.This experimental method is highly valuable for investigating the mechanical properties of rocks.

The well logging data provides a reliable way to reach the aim with respect to the drillability of a well (Tokle et al. 1986; Onyia 1988; Khaksar et al. 2009; Kumar and Rao 2012). Previous studies showed that petrophysical properties such as electrical, acoustic, and radioactive parameters measured by downhole well logging tools are related with the rock's compressive strength, and can be used to obtain the compressive strength. These methods can be classified as: (1) Direct regressions with acoustic velocity, resistivity, density, as well as radioactive intensity (Chang 2004; Chang et al. 2006; Olea et al. 2008; Sharma et al. 2010; Najibi et al. 2015; Xu et al. 2016; Abbas et al. 2018); (2) Indirect regressions with some geological and formation parameters interpreted from well logging data such as porosity, shale content, water saturation, surface area, grain size, and elastic modulus (Talesnick et al. 2001; Agustawijaya 2007; Nadah et al. 2013; Dewhurst et al. 2015; Silva et al. 2015; Kitamura and Hirose 2017; Yang et al. 2017; Farrokhrouz and Asef 2017; Hashiba et al. 2019); (3) Statistical or machine learning techniques such as support vector regression, grey forecasting model, genetic algorithm, artificial neural network, and gene expression programming (Rafiai and Jafari 2011; Rabbani et al. 2012; Cabalar et al. 2012; Liu et al. 2015; Zingg et al. 2016; Babanajad et al. 2017; Asadi 2017; Hassanvand et al. 2018; Vapnik et al. 2018; Kandiri et al. 2020). However, these methods mentioned above have obvious deficiencies: (1) The empirical equations are developed in terms of specific study and rock type, which are strongly lithological dependent; (2) The precise petrophysical parameters such as porosity, mineral content, and surface area are very difficult to obtain in unconventional formations such as gas shale and tight sand; (3) The influence of the grain size, microstructure, pore geometry, and pore size distribution on the compress strength is still not completed investigated (Forquin et al. 2008; Heap et al. 2014; Baud et al. 2014; Shen and Shao 2016; Bubeck et al. 2017; Griffiths et al. 2017; Farid et al. 2017).

NMR measurement uses the established CPMG pulse sequence to obtain the transverse T_2 relaxation time distribution. Provide sensitivity to pore geometry or fluid phase (i.e. oil, brine and gas) when hydrogen-containing liquid is present.The low field nuclear magnetic resonance (NMR) technique is featured as lithology-independent and non-invasive, which provides formation properties such as porosity, permeability, fluid saturation, and pore size distribution. The low field NMR measurement can be performed both in laboratory analysis and in field exploration.

It is more convenient for the core-log calibration compared with other pore geometry characterization methods such as scanning electron microscopy (SEM) and X-ray computed tomography (X-CT) (Lou et al. 2018; Heap et al. 2014; Farid et al. 2017; Yang et al. 2019). This method has been applied to study rock's elastic properties, geomechanical behaviors, as well as the strength and deformation characteristics (Zhai et al. 2017; Yang et al. 2018; Li et al. 2019; Ge et al. 2020). The aim of the research is to investigate the relationship between the pore size distribution and the compressive strength of the tight reservoir using the NMR measurement, to recognize the contribution of different pore ranges on the rock's strength characteristics. In additional, the conventional parameters such as porosity, mineral content, static and dynamic elastic modulus, as well as acoustic velocity

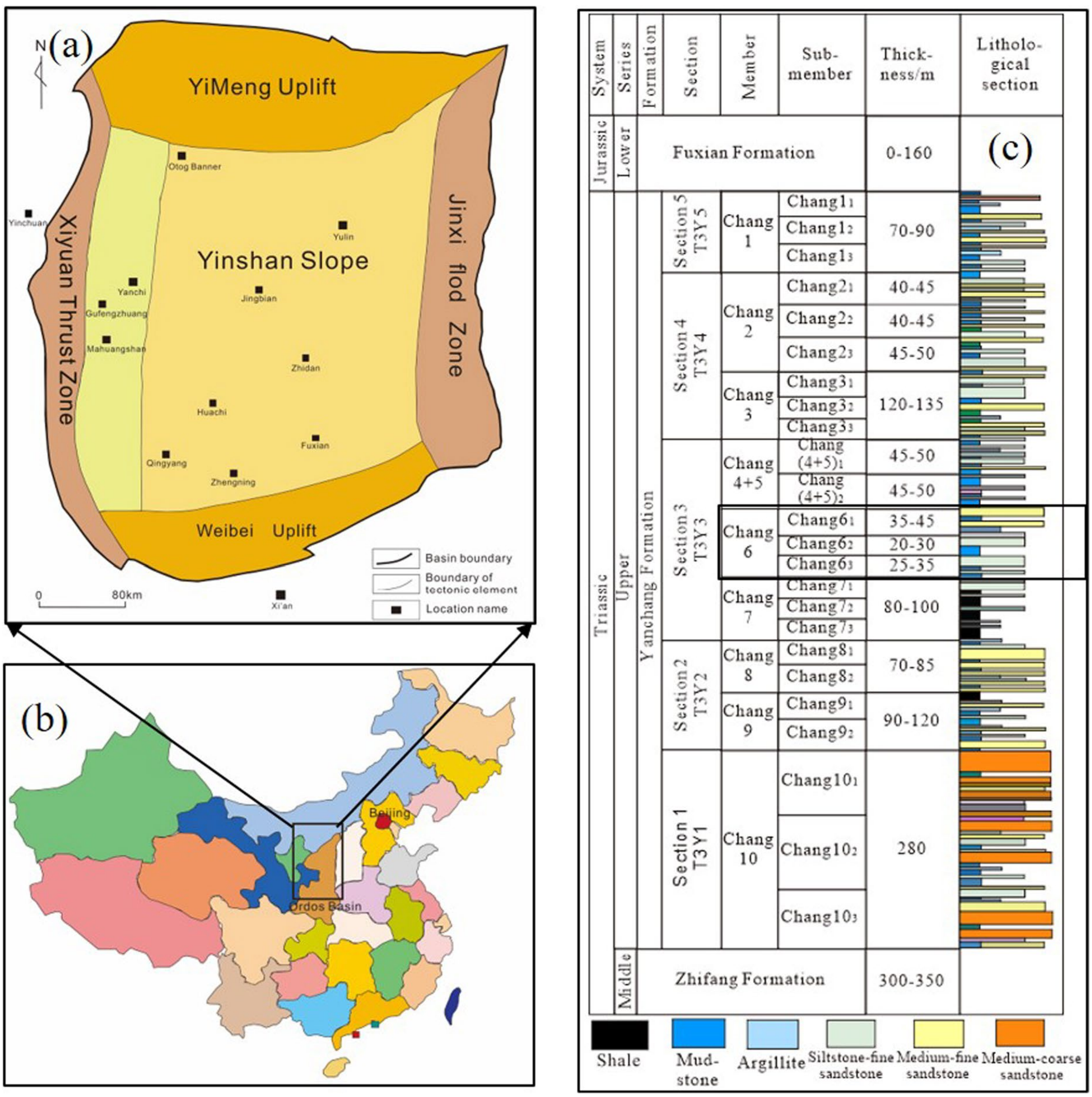

Fig. 1 Location, tectonic division and stratigraphic sequence division of the Triassic Yanchang Formation of Mahuangshan area in the Ordos Basin

are also measured during the experiment. We hope the research finding can provide more comprehensive recognitions on the impact of the compressive strength besides the rock matrix.

2 Materials and experiments

2.1 Geological background and pretreatment

Mahuangshan area is belonged to the Yanchi County, Ningxia Hui autonomous region of China, as seen in Fig. 1. It is located in the central Tianhuan Depression of Ordos basin. Chang 6 Formation is the main oil production reservoir with the thickness ranges from 80 to 110 m. It is a typical delta deposit, developed mainly with grey-green fine grain sandstone, siltstone, and dark mudstone. 12 samples from two wells are collected for our experiments. These samples are reshaped and polished to cylindrical plungers with the diameter of approximate 2.5 cm and the length of 4.5–5 cm. They are put in to an oil-cleaning instrument at the temperature of 90 centigrade for 10 days to remove the remnants of the original fluids and the invaded drilling mud. Then, they are moved to an oven with the temperature and time of 95 centigrade and 24 h, respectively, to ensure that there is no fluid in the pore space. We measure the density, gas filled porosity, and gas permeability for these dried samples. They are performed by XP205 analytical balance, UltraPoreTM-300 helium pycnometer system (Corelab Incorporation), and UltraPeamTM-400 helium permeability system (Corelab Incorporation). Next, they are saturated with sodium chloride solution with the salinity of 90 g/L, which is equivalent with the formation water. It is performed by an auto-saturating container, with the saturating duration and confining pressure of 48 h and 20 MPa, to ensure the completely saturation state. The water saturated porosity is obtained using the Archimedes' principle. Acoustic velocities, NMR relaxation spectrums are conducted for fully saturated samples. NMR spectrums of irreducible water saturated samples are also collected. They are saturated again to conduct the pseudo-triaxial compression test. Lastly, they are crushed into powders for X-ray diffraction (XRD) analysis by AXS D8 advance X-Ray diffractometer (Bruker Incorporation). Types and contents of minerals and clays can be extracted easily.

2.2 Low field NMR measurement

We use MARAN-II ultra-rock spectrometer (Oxford Instrument Incorporation) with an approximate main frequency of 2 MHz, to perform NMR measurements. The experiments are conducted in CNPC key well logging laboratory. To ensure the maximal acquisition of all hydrogen-related signals and the data quality, the acquisition parameters are as follows: the waiting time is 6 s, the echo spacing is 0.2 ms, the of scan number is 256, the receiving gain is 80%, and the echo number is 8192. The pulse sequence used is the conventional Carr-Purcell-Meiboom-Gill (CPMG) pulse sequence. The measured decaying signals are then inverted into the transversal relaxation (T_2) spectrums with the WinDXP software package.

As is known, the low field NMR measures the transversal relaxation of the spins in porous rocks, where the total signal intensity or the spectrum amplitude can be calibrated to the porosity of the sample. Details on the workflow of the calibration were addressed in many articles (Ge et al. 2023; Xu et al. 2015; Xiao et al. 2012). In our measurement, we used the standard samples with known porosity values to establish the calibration equation between the porosity and the normalized initial echo amplitude. Then, the porosity of the real core samples can be obtained conveniently. The linear calibration equation is expressed as,

$$\phi_{NMR} = m \times S + n \tag{1}$$

where ϕ_{NMR} is the porosity calibrated by the NMR measurement; S is the normalized initial echo amplitude by the CPMG pulse sequence; m and n are calibration constants.

Besides the porosity, the cutoff value of the transversal relaxation time (T_2c) is also a very important parameter obtained by the low field NMR measurement. It is generally used to divide the entire T_2

spectrum into two categories. The fluids in pores with T_2 value higher than T_2c are movable and vice versa. The parameter is often obtained by the comparison between the fully saturated T_2 spectrum and the irreducible saturated T_2 spectrum. details on the cutoff value were addressed by many authors (Ge et al. 2015; Chen et al. 2023; Testamanti and Rezaee 2017).The bound water saturation in core samples refers to the percentage of water in the rock that is immobilized because it is trapped by the particles or mineral surfaces of the rock. This portion of water cannot flow freely and constitutes the non-mobile water within the total porosity. The movable water in the core can be separated and only bound water can be left in the core by centrifugal experiment at a certain speed on the completely saturated water sample.Therefore, the bound water saturation can be calculated by the nuclear magnetic experiment data after completely saturated water and centrifugation.

2.3 The pseudo-triaxial compression and the acoustic measurement

The pseudo-triaxial compression tests were performed by Autolab 1500 (New England Research Incorporation) in CNPC key well logging laboratory. The confining pressure is 39 MPa, and the temperature is 30 degrees Celsius. The axial stress, axial strain and radial strain are recorded during the pressure loading process. Therefore, the static elastic parameters such as Young's modulus, the shear modulus, the bulk modulus, the Poisson's ratio, as well as the compressive strength can be computed by Chinese National Standard 'Methods for determining the physical and mechanical properties of coal and rock-Part 9: Methods for determining the triaxial strength and deformation parameters of coal and rock (GB/T 23561.9–2009).

The dynamic elastic parameters such as the Young's modulus, shear modulus, bulk modulus, Poisson's ratio are computed by the acoustic velocities and the density. There are expressed as follows,

$$E_d = \frac{\rho V_s^2\left(3V_p^2 - 4V_s^2\right)}{V_p^2 - V_s^2} \tag{2}$$

$$S_d = \rho V_s^2 \tag{3}$$

Table 1 Basic petrophysical parameters for these samples

Sample number	Gas porosity (%)	Brine porosity (%)	NMR porosity (%)	Gas permeability (mD)	Bulk density (g/cm^3)	P wave velocity (m/s)	S wave velocity (m/s)
1	9.70	9.37	9.22	0.203	2.53	4539.34	2713.63
2	7.98	7.61	7.49	0.064	2.57	4821.23	3058.80
3	7.84	7.50	7.34	0.132	2.57	4787.07	2812.67
4	13.54	13.14	12.80	0.451	2.46	3956.63	2220.05
5	4.00	3.51	3.69	0.039	2.63	5126.37	3084.93
6	5.24	4.66	4.97	0.071	2.60	4940.54	2970.00
7	12.93	12.77	12.45	0.485	2.47	3959.90	2179.73
8	14.87	14.71	14.19	0.738	2.42	3924.70	2172.48
9	12.82	12.63	12.31	0.434	2.46	4123.54	2360.58
10	15.55	15.24	14.85	0.961	2.43	3874.83	2089.64
11	6.84	6.34	6.42	0.058	2.57	4960.92	2782.25
12	10.10	9.64	9.54	0.105	2.52	4560.25	2730.55

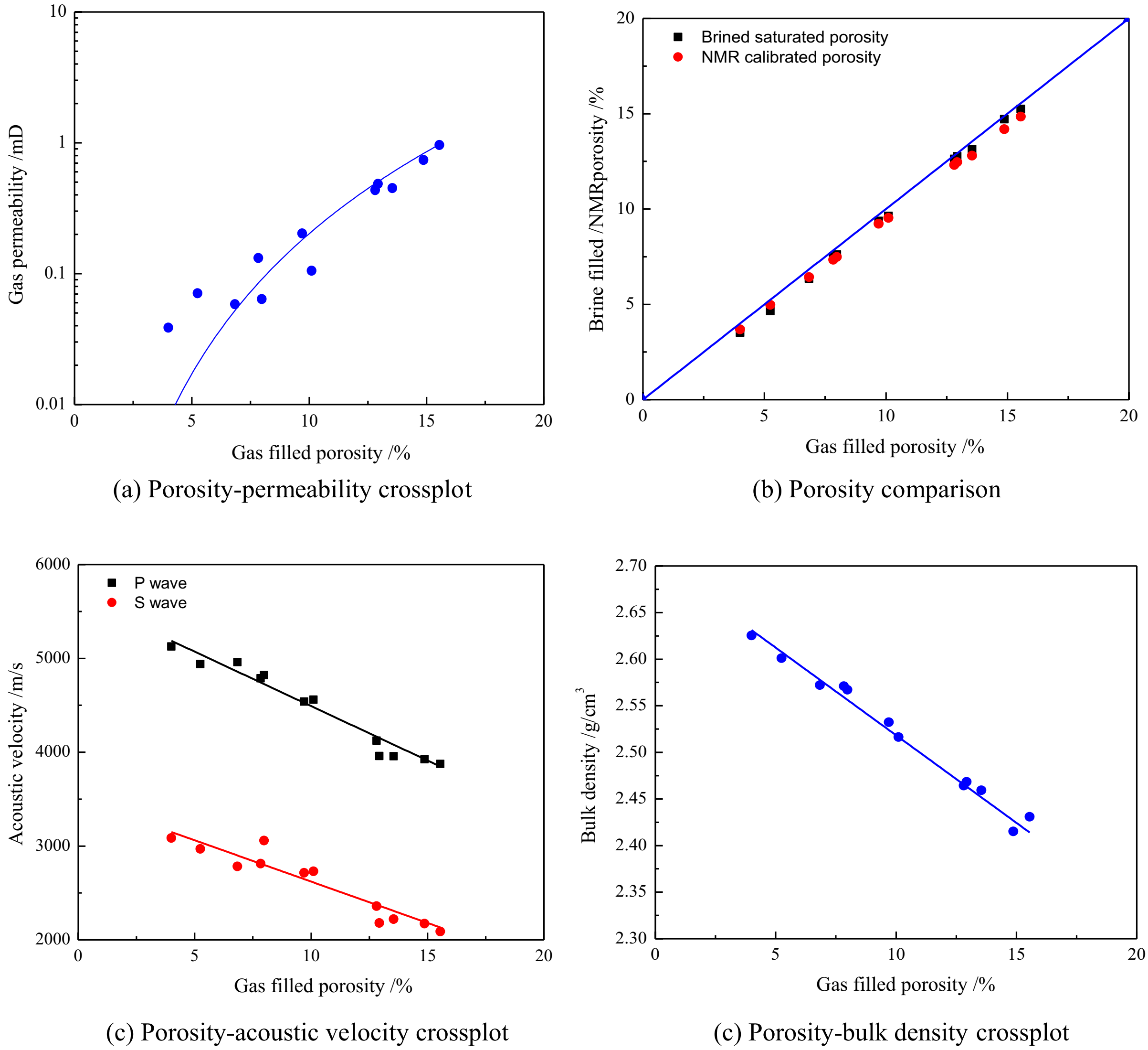

(a) Porosity-permeability crossplot

(b) Porosity comparison

(c) Porosity-acoustic velocity crossplot

(c) Porosity-bulk density crossplot

Fig. 2 Porosity comparisons and their relationships with permeability, acoustic velocity, and density

$$V_d = \rho\left(V_p^2 - \frac{3V_s^2}{4}\right) \tag{4}$$

$$P_d = \frac{V_p^2 - 2V_s^2}{2\left[\left(V_p^2 - V_s^2\right)\right]} \tag{5}$$

where V_p and V_s are compressive velocity and shear velocity, respectively; ρ is the density of the rock.

3 Results and discussion

3.1 Basic petrophysical properties

The basic petrophysical parameters are shown in Table 1 and Fig. 2. It is seen that the gas filled porosity ranges from 4% to 15.55%, and the gas permeability ranges from 0.04mD to 0.96mD, lower than conventional reservoirs. The permeability is generally increased with the porosity, but simple regression is

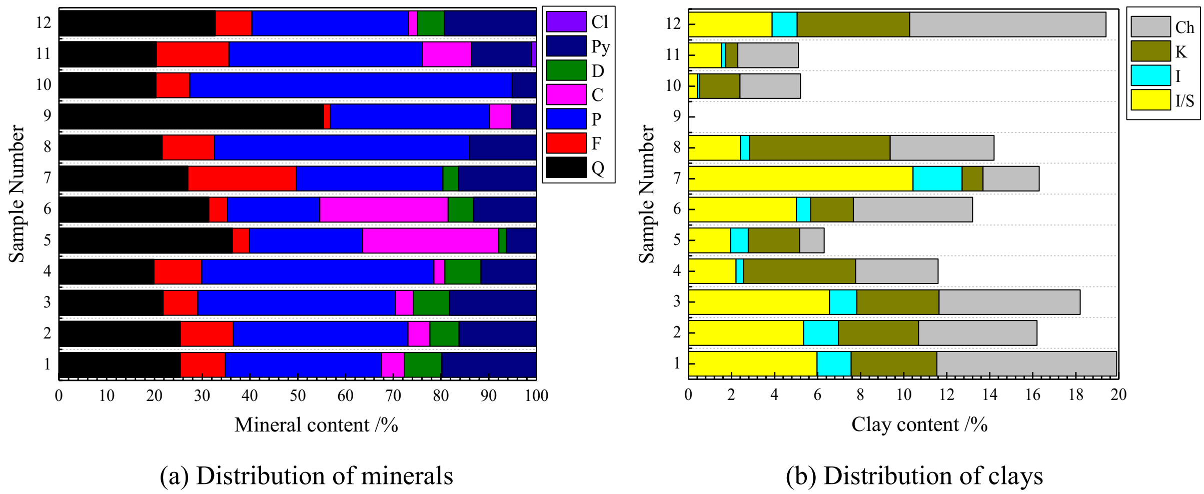

Fig. 3 Distribution of minerals and clays observed by XRD analysis (*Q* quartz, *F* K-feldspar, *P* plagioclase, *C* calcite, *D* dolomite, *Py* pyrite, *Cl* clay, *I/S* illite–smectite mixed layer, *I* illite, *K* kaolinite, *Ch* chlorite)

Table 2 Mineralogical composition for these samples

Sample number	Quartz (%)	K-feldspar (%)	Plagioclase (%)	Calcite (%)	Dolomite (%)	Clay (%)	Pyrite (%)
1	25.40	9.40	32.70	4.80	7.90	19.90	–
2	25.40	11.10	36.60	4.60	6.10	16.20	–
3	21.80	7.30	41.30	3.80	7.60	18.20	–
4	19.90	10.00	48.60	2.30	7.60	11.60	–
5	36.30	3.60	23.70	28.50	1.60	6.30	–
6	31.40	3.90	19.30	26.90	5.30	13.20	–
7	27.00	22.70	30.70	–	3.30	16.30	–
8	21.60	11.00	53.30	–	–	14.20	–
9	55.40	1.40	33.40	4.60	–	5.20	–
10	20.30	7.10	67.50	–	–	5.10	–
11	20.40	15.20	40.50	10.30	–	12.50	1.10
12	32.70	7.70	32.80	1.90	5.60	19.40	–

difficult to fitting the permeability. The brine saturated porosity, NMR calibrated porosity is generally in accordance with the gas filled porosity, indicating that the pores are fully saturated with water and good performance of NMR measurements. In additional, the compressive wave (P wave) velocity, the shear wave (P wave) velocity, and the bulk density show favorable linear relationships with the porosity, indicating that the velocity and density for the rock matrix is stable.

Figure 3 gives the absolute content of minerals and clays observed by XRD analysis. It is seen that the rock matrix is mainly composed by quartz, K-feldspar, plagioclase, and clay, but their contents vary broadly. Moreover, the clay is mainly composed by illite–smectite mixed layer and chlorite. Due to the heterogeneous development of these minerals, it is difficult to obtain their contents and spatial distribution via conventional well logging data. The detailed experiment results of the mineralogical

Table 3 Absolute clay composition for these samples

Sample number	Illite–smectite mixed layer (%)	Illite (%)	Kaolinite (%)	Chlorite (%)	Illite/smectite ratio
1	5.97	1.59	3.98	8.36	10
2	5.35	1.62	3.73	5.51	10
3	6.55	1.27	3.82	6.55	10
4	2.20	0.35	5.22	3.83	10
5	1.95	0.82	2.39	1.13	10
6	5.02	0.66	1.98	5.54	10
7	10.43	2.28	0.98	2.61	10
8	2.41	0.43	6.53	4.83	10
9	–	–	–	–	–
10	0.42	0.10	1.87	2.81	10
11	1.53	0.20	0.56	2.81	10
12	3.88	1.16	5.24	9.12	10

and clay distributions are shown in Tables 2 and 3, respectively.

3.2 NMR T_2 spectrums

Figure 4 show NMR spectrums for samples at different saturating states. It is seen that most spectrums for fully water saturated samples are mono-modal distributed but the peak position ranges from 4 to 100 ms. The shape of spectrums for irreducible water saturated samples is similar to fully water saturated samples and the left part remains unaltered, whereas the right part is decreased. It is easy to interpret since the low relaxation time is corresponded to the small pore radius. Table 4 summarized the geometric mean (T_2gm) and the arithmetic mean (T_2am) of fully water saturated and irreducible water saturated samples, the cutoff value (T_2c), the movable water saturation (Swm), as well as the irreducible water saturation (Swi). We can conclude that T_2am is positively correlated with T_2gm for samples under the fully saturated state. However, there is no obvious correlation between T_2am and T_2gm for samples under the irreducible water saturated state. T_2c is generally lower than 13 ms and ranges from 3 to 13 ms, revealing that a dynamic value is more reasonable.

It is should be noted that both the geometric mean (T_2gm) and the arithmetic mean (T_2am) are expressed as,

$$T_{2gm} = \sqrt[\sum_{i=1}^{p} f_i]{\prod_{i=1}^{p} T_{2i}^{f_i}} \tag{6}$$

$$T_{2am} = \frac{\sum_{i=1}^{p} T_{2i} f_i}{\sum_{i=1}^{p} f_i} \tag{7}$$

where f_i is the amplitude for the corresponding T_{2i}; p is the total number of the T_2 spectrum.

Physically, the geometric mean is used to describe the concentration degree of the T_2 spectrum and the arithmetic mean is used to describe the average position of the T_2 spectrum (Xiao et al. 2018).

3.3 Geomechanical behaviors

Figure 5 show the time-dependent axial stress, the axial strain, the radial strain, and the volumetric strain of samples during the pressure loading stage. It is seen that the stress–strain response is complicated. Some samples with similar petrohysical properties and mineralogical compositions behave significant differences in geomechanical properties. Table 3 and Fig. 6 summarizes the static and dynamic geomechanical parameters and their interrelationships for these samples obtained from stress–strain relationships and acoustic measurements. It is observed that

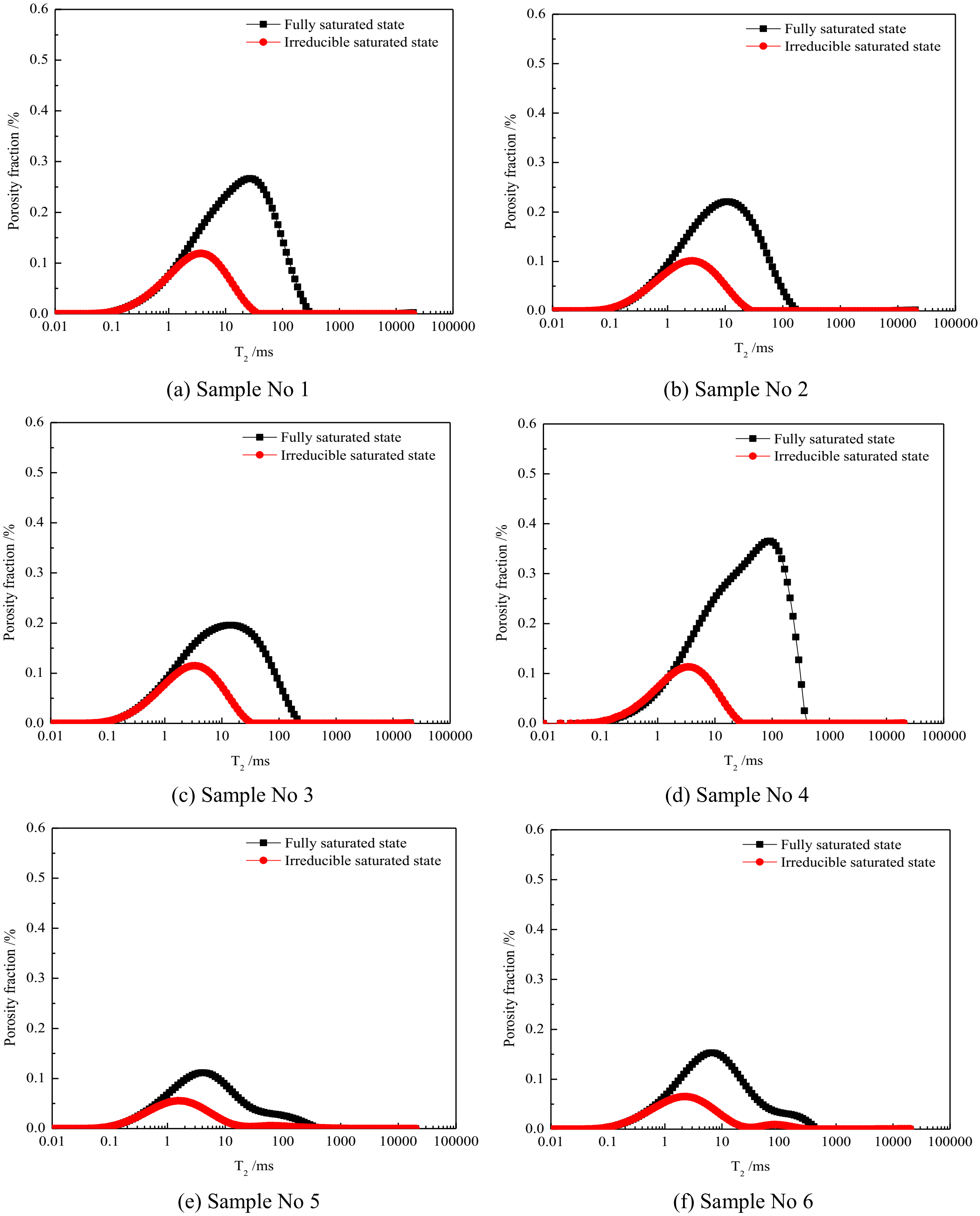

Fig. 4 NMR T_2 spectrums for samples under the fully water saturated state and the irreducible water saturated state

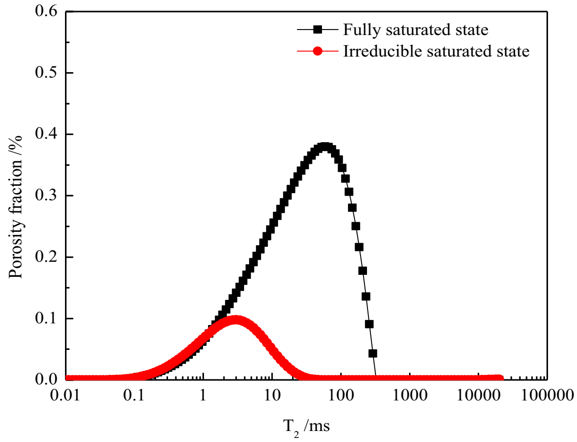

(g) Sample No 7

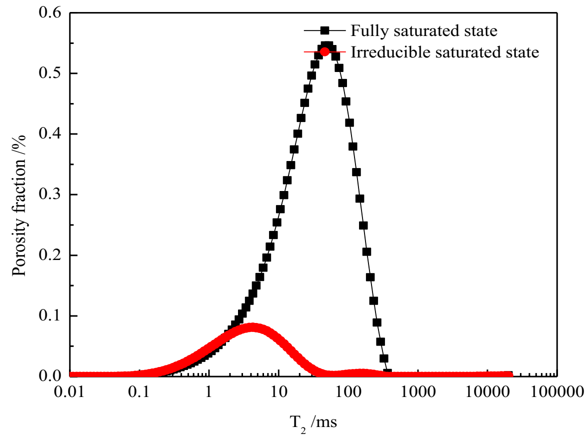

(h) Sample No 8

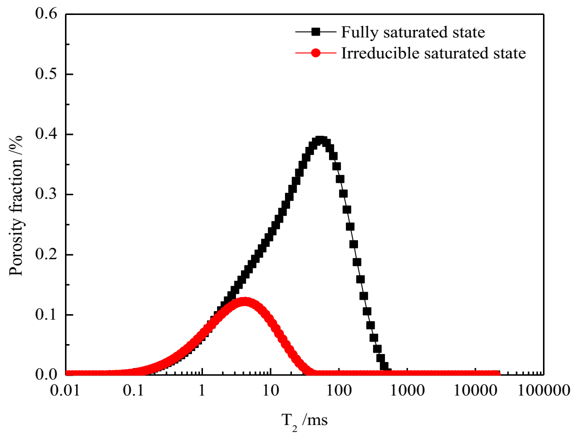

(i) Sample No 9

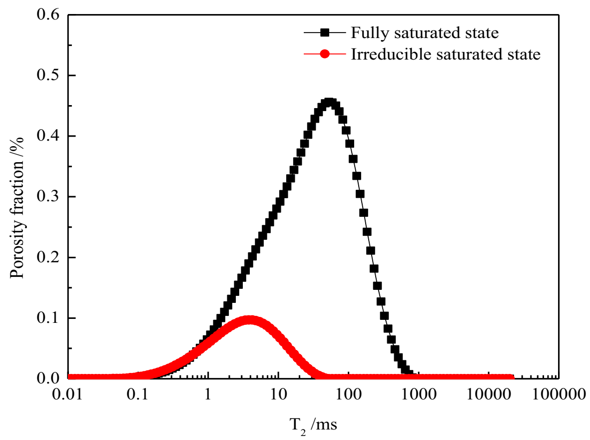

(j) Sample No 10

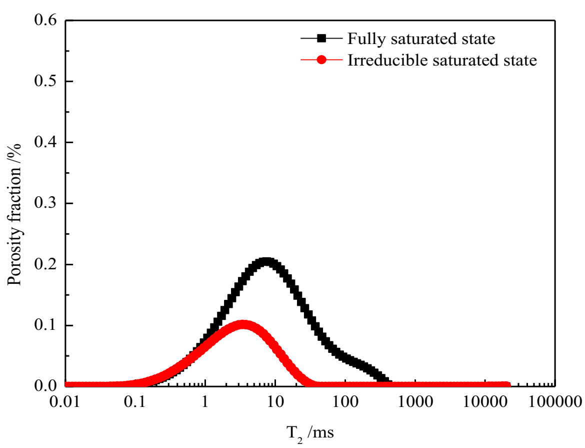

(k) Sample No 11

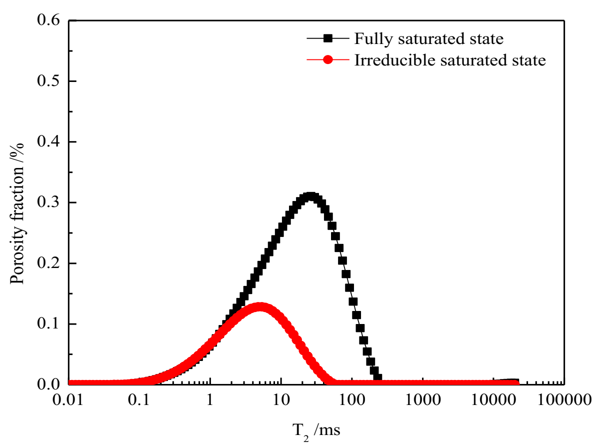

(l) Sample No 12

Fig. 4 (continued)

Table 4 NMR parameters for these rock samples

Sample number	T_2gm saturated (ms)	T_2am saturated (ms)	T_2gm irreducible (ms)	T_2am irreducible (ms)	T_2c (ms)	Swi (%)	Swm (%)
1	12.47	46.75	2.65	4.71	6.77	34.00	66.00
2	7.11	40.68	2.01	3.58	4.26	36.41	63.59
3	8.77	33.59	2.50	18.24	6.33	41.52	58.48
4	24.31	60.33	2.53	17.04	6.67	22.51	77.49
5	4.84	18.61	1.93	13.11	3.08	42.09	57.91
6	6.77	23.31	2.39	46.41	3.87	37.50	62.50
7	22.09	50.87	2.34	32.53	5.59	19.90	80.10
8	28.39	58.21	3.52	52.75	7.35	15.71	84.29
9	22.67	55.90	3.06	5.38	8.14	25.57	74.43
10	25.16	62.70	2.92	5.33	5.20	17.53	82.47
11	7.74	23.05	2.59	19.83	5.18	41.06	58.94
12	13.66	54.73	3.65	6.72	9.03	36.57	63.43

the static Young's modulus and static shear modulus are generally higher, and are positively correlated with their dynamic values. However, the static volumetric modulus and Poisson's ratio are generally lower than dynamic values and show no clear correlations (Table 5).

3.4 Pore size and component control on the compressive strength

Figure 7 gives the correlations of the compressive strength (CS) and NMR parameters including T_2gm, T_2am, Swi, Swm, T_2c, and NMR porosity. It is seen that the compressive strength is decreased with the increase of T_2gm and T_2am for core samples under the fully water saturated state. This phenomenon indicates that rock's strength is controlled by the pore size. Rock samples with larger pore radius are easier to reach the failure state. It seems that there is no clear relationship between the compressive strength and the T_2gm and T_2am for samples under the irreducible water saturated state. It is easy to be interpreted since the NMR response of irreducible water saturated rock sample is mainly contributed by clay bound water and capillary bound water, which cannot be used to characterize the pore size distribution of all ranges. Moreover, it is observed that the compressive strength is positively correlated with the irreducible water saturation, whereas negatively correlated with the movable water saturation, suggesting that the compressive strength is mainly controlled by the pore distribution. The rock is easier to be fractured for higher percentage of movable fluids, which are often resided in larger pores. We also exam the influence of T_2 cutoff values and NMR porosity on the compressive strength, as is shown in Fig. 7e, f. It is seen that the compressive strength is weakly decreased with the increase of the cutoff value, although the physical explanation is not understood. In additional, the compressive strength is negatively correlated with the NMR obtained porosity, which is similar to most of previous publications.

Based on the discussion, it is practical for us to establish the model to predict the compressive strength using the NMR obtained parameters, which can be expressed as,

$$CS = a \times T_{2gm} + b \times \phi_{NMR} + c \quad (8)$$

where a, b, c are fitting parameters, which may vary in different regions. In this study, they are − 1.583, − 12.292, 320, respectively. The correlation coefficient is as high as 0.92. We did not recommend to use the irreducible water saturation and the

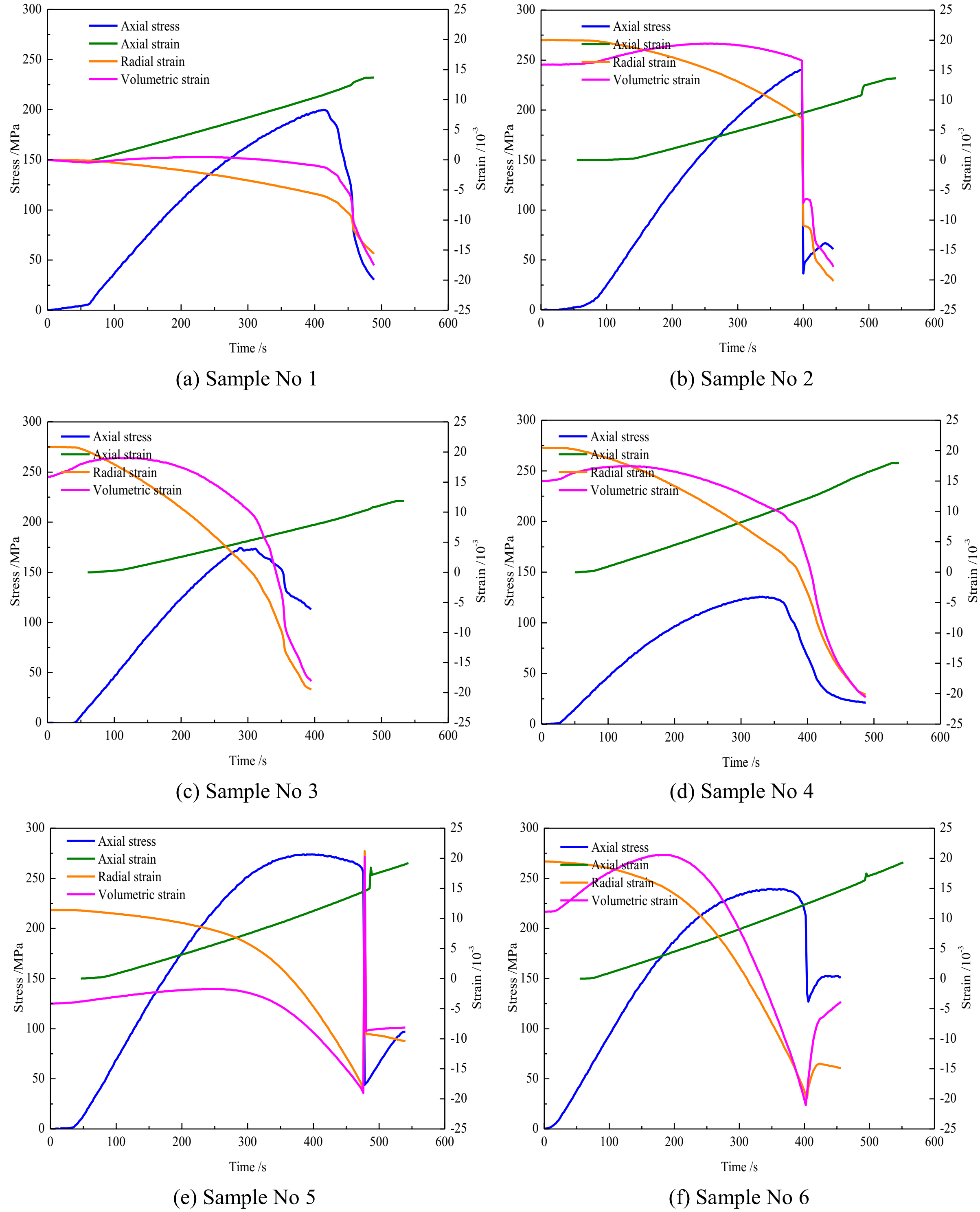

Fig. 5 Time-dependent axial stress, axial strain, as well as radial strain for fully water saturated samples

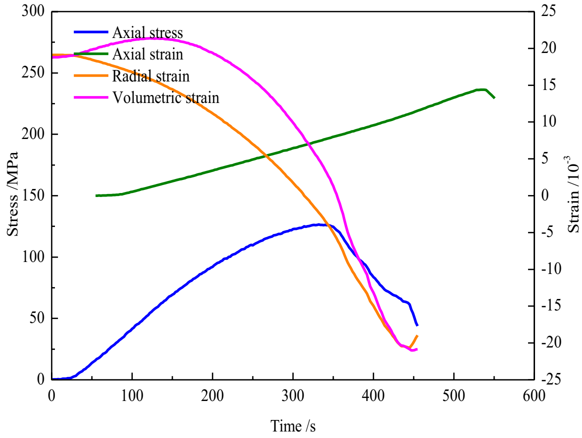

(g) Sample No 7

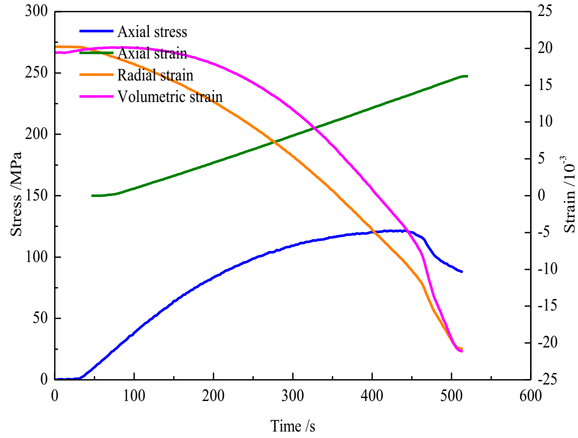

(h) Sample No 8

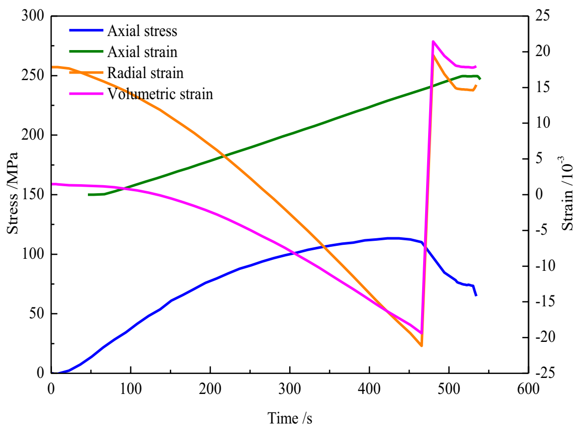

(i) Sample No 9

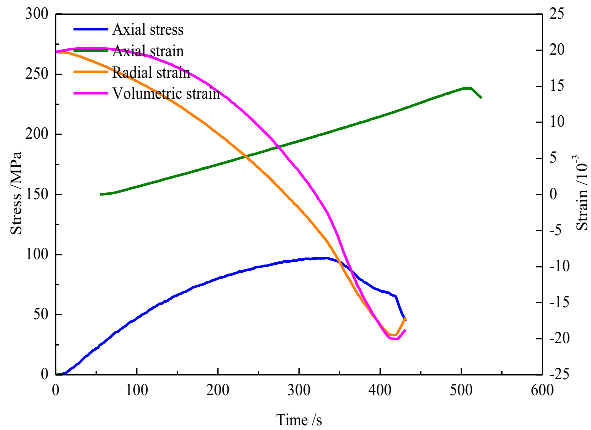

(j) Sample No 10

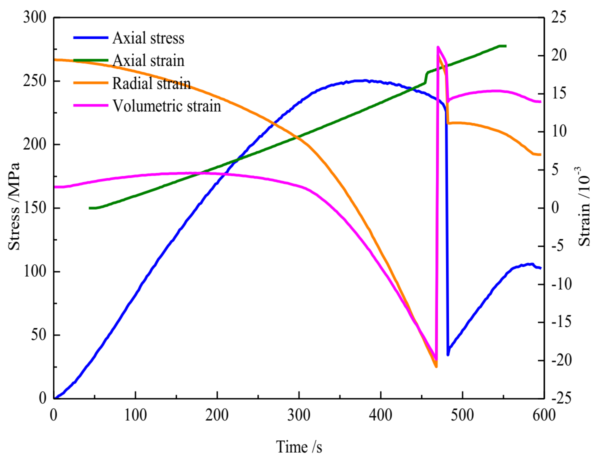

(k) Sample No 11

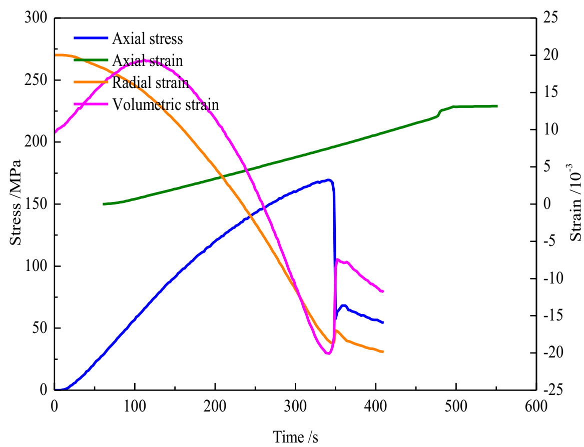

(l) Sample No 12

Fig. 5 (continued)

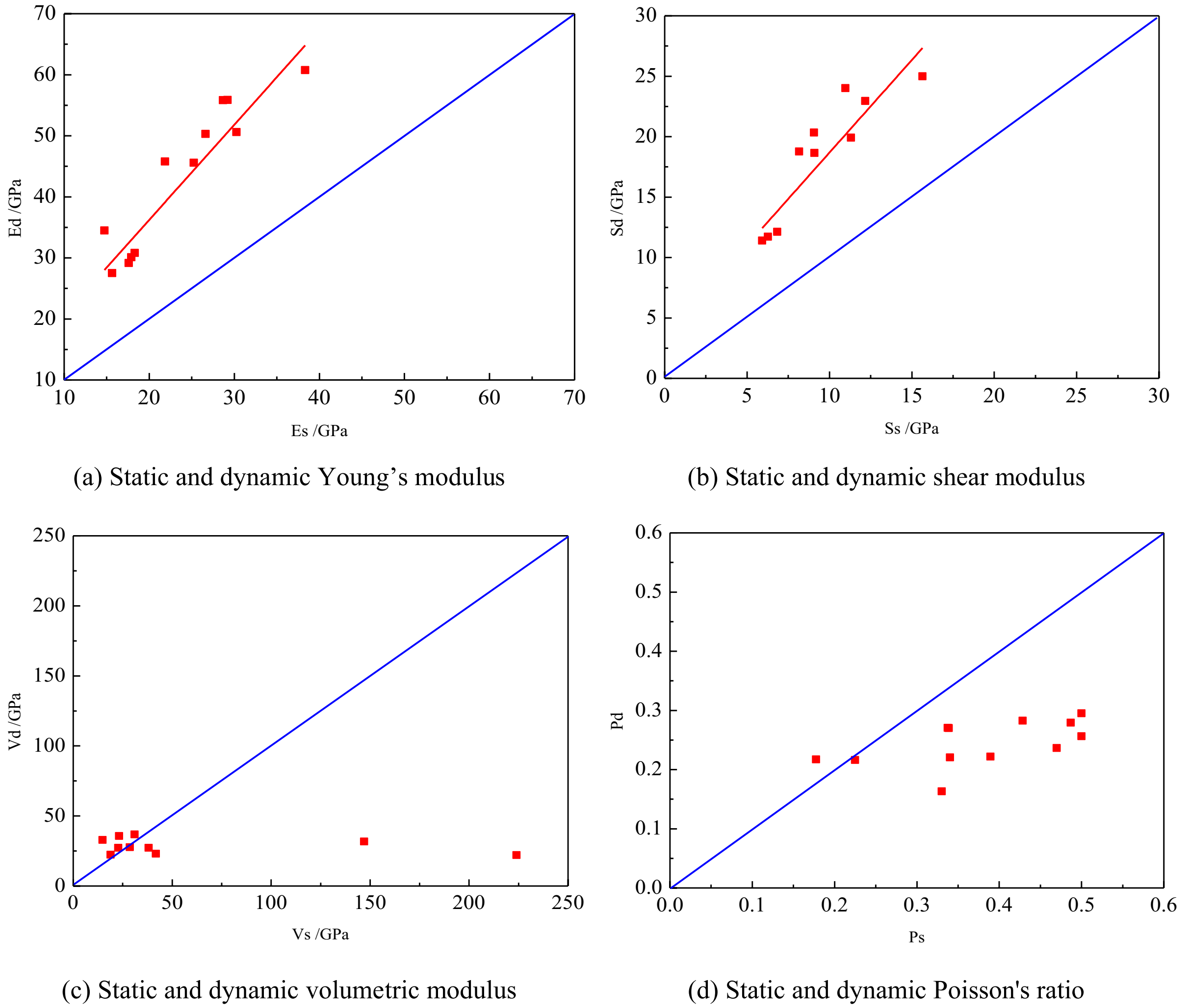

Fig. 6 Relationship between static and dynamic geomechanical parameters

movable water saturation for the regression since both are difficult to obtain by fully saturated spectrums.

We re-exam the relationship between the compressive strength and mineral compositions, as shown in Fig. 8. It seems that there are no clear correlations between the compressive strength and the mineral contents expect for the plagioclase. The result indicates that plagioclase may be the brittle mineral in the studied region. The empirical equation can be expressed as,

$$CS = d \times V_{plagioclase} + e \tag{9}$$

where d and e are fitting parameters. In this study, they are − 2.942 and 290.58. The correlation coefficient for this fitting is as low as 0.39.

Figure 9 gives the comparison between two different methods. It is seen that the precision obtained from the direct regression between the compressive strength and the plagioclase content is relative lower than the result obtained by the NMR parameters.

Table 5 Static and dynamic geomechanical parameters for fully water saturated samples

Sample number	CS (MPa)	Static geomechanical parameters				Dynamic geomechanical parameters			
		Es (Gpa)	Ss (Gpa)	Vs (GPa)	Ps	Ed (Gpa)	Sd (Gpa)	Vd (GPa)	Pd
1	199.8	25.3	9.1	38.1	0.39	45.6	18.6	27.3	0.22
2	240.1	29.2	11.0	28.7	0.33	55.9	24.0	27.6	0.16
3	174.3	26.6	9.1	147.0	0.47	50.3	20.3	31.8	0.24
4	125.8	18.3	6.8	18.9	0.34	30.8	12.1	22.3	0.27
5	274.0	38.3	15.6	23.2	0.22	60.8	25.0	35.7	0.22
6	239.5	28.7	12.2	14.8	0.18	55.8	22.9	32.9	0.22
7	126.6	17.9	6.3	41.8	0.43	30.1	11.7	23.1	0.28
8	121.4	17.6	5.9	224.0	0.49	29.2	11.4	22.0	0.28
9	113.3	14.7	–	–	0.50	34.5	13.7	23.6	0.26
10	97.1	15.7	–	–	0.50	27.5	10.6	22.3	0.29
11	250.5	30.3	11.3	31.0	0.34	50.6	19.9	36.8	0.27
12	169.5	21.9	8.2	22.8	0.34	45.8	18.8	27.3	0.22

Moreover, it is very difficult to obtain the plagioclase content because they are no direct well logging measurements to detect the minerals' compositions and their contents, expect the elemental capture spectroscopy (ECS) logging.

4 Conclusions

We investigated the relationship between the pore size and the compress strength for tight sandstone based on laboratory NMR measurements and pseudo-triaxial compression tests, aiming to develop an effective way to predict the compressive strength using the NMR data. The main conclusions are as follows:

1. The rock's strength is controlled by the pore size distribution for tight sandstone with similar minerals' compositions. The rock is easier to easier to reach the failure state for larger average pore radius, supported by the observation between the compressive strength and the geometric, as well as the arithmetic mean of the transversal relaxation time.
2. The rock's strength is influenced by the fluid distribution state. The compressive strength is positively correlated with the irreducible water saturation, but negatively correlated with the movable water saturation. The rock is easier to be fractured with the increase of the percentage of larger pores and movable fluids. The rock is easier to be fractured for higher percentage of movable fluids, which are often resided in larger pores.
3. There are weak correlations between the compressive strength and the mineral contents, indicating that the rock's strength estimated by brittle minerals may be invalid.
4. The compressive strength for water saturated samples can be predicted precisely through multiple regressions with NMR parameters such as T_2gm and porosity. The empirical equation can be potentially used for geophysical prospecting with NMR logging data.

It is noted that our observations are limited to laboratory studies of tight sandstone, much work should be done to further investigate their relationships. Moreover, the fluid phases and their distributions under the reservoir condition should be considered

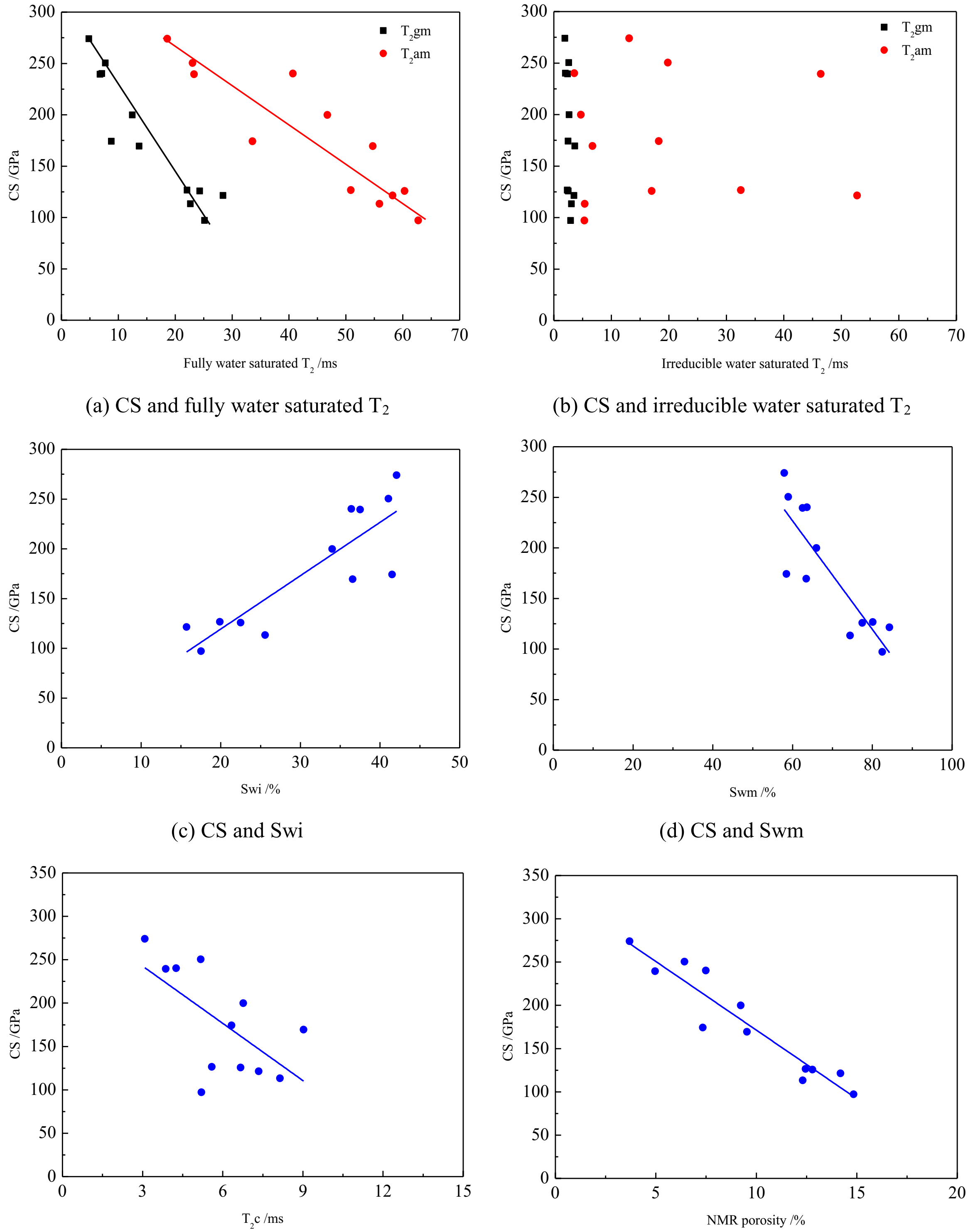

(a) CS and fully water saturated T_2

(b) CS and irreducible water saturated T_2

(c) CS and Swi

(d) CS and Swm

(e) CS and T_2c

(f) CS and NMR porosity

Fig. 7 Relationship between the compressive strength and NMR parameters

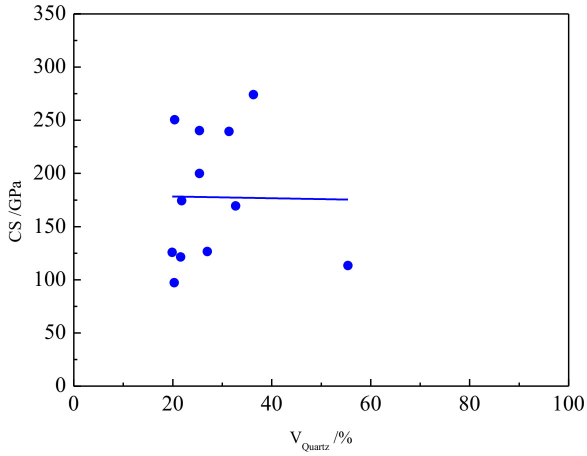

(a) CS and quartz content

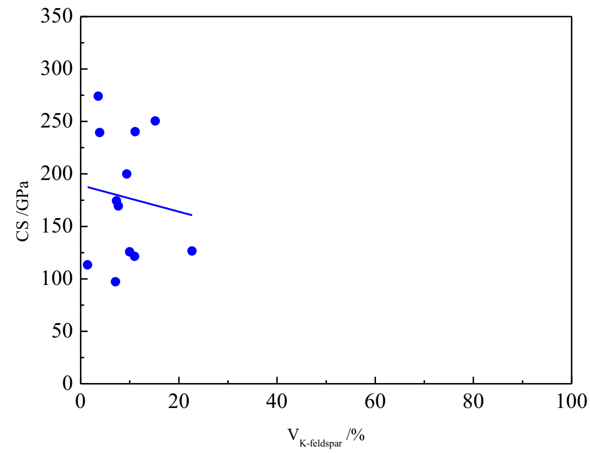

(b) CS and K-feldspar content

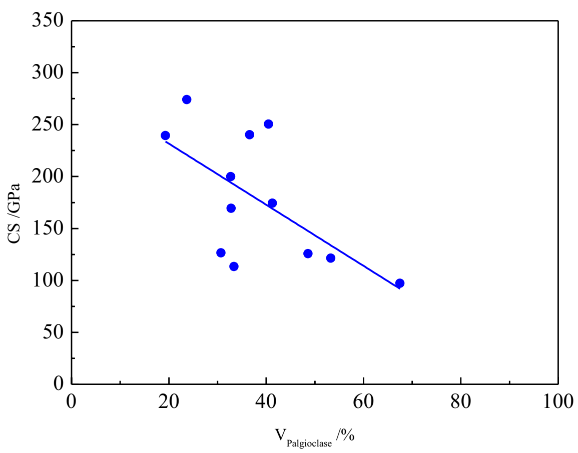

(c) CS and plagioclase content

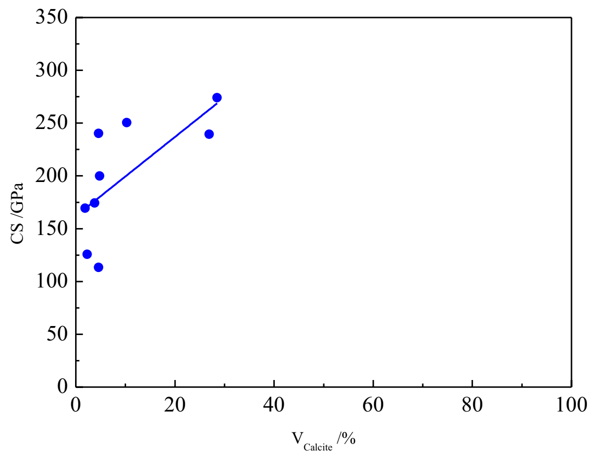

(d) CS and calcite content

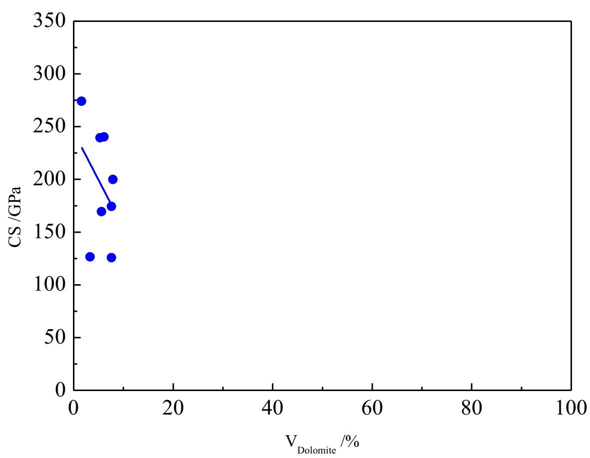

(e) CS and dolomite content

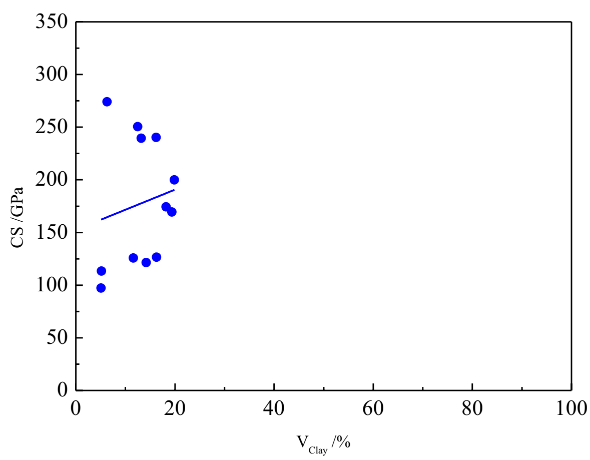

(f) CS and clay content

Fig. 8 Relationship between the compressive strength and the mineral composition

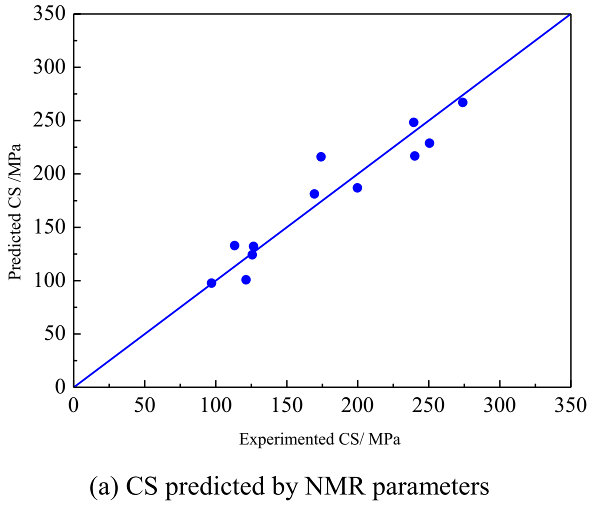

Fig. 9 Comparison between the experimented and predicted compressive strength

since the pore is not only wetted by the single water phase.

Acknowledgements This work was supported by Natural Science Foundation of Shandong Province (ZR2023YQ034), the National Natural Science Foundation of China (42174142), CNPC Innovation Found (2021DQ02-0402), and CNPC Science and Technology Project (2021DJ3804).

Availability of data and materials The datasets and materials used and/or analyzed during the current study are available from the corresponding author on reasonable request.

Declarations

Competing interests We declare that we have no financial and personal relationships with other people or organizations that can inappropriately influence our work, there is no professional or other personal interest of any nature or kind in any product, service and/or company that could be construed as influencing the position presented in, or the review of, the manuscript entitled "Predicting the compressive strength of tight sandstone based on the low field NMR and pseudo-triaxial compression measurements".

References

Abbas A, Flori R, Alsaba M (2018) Estimating rock mechanical properties of the Zubair shale formation using a sonic wireline log and core analysis. J Nat Gas Sci Eng 53:359–369

Agustawijaya D (2007) The uniaxial compressive strength of soft rock. Civil Eng 9(1):9–14

Asadi A (2017) Application of artificial neural networks in prediction of uniaxial compressive strength of rocks using well logs and drilling data. Procedia Eng 191:279–286

Babanajad S, Gandomi A, Alavi A (2017) New prediction models for concrete ultimate strength under true-triaxial stress states: an evolutionary approach. Adv Eng Softw 110:55–68

Baud B, Wong T, Zhu W (2014) Effects of porosity and crack density on the compressive strength of rocks. Int J Rock Mech Min 67:202–211

Bubeck A, Walker R, Healy D, Dobbs M, Holwell D (2017) Pore geometry as a control on rock strength. Earth Planet Sc Lett 457:38–48

Cabalar AF, Cevik A, Gokceoglu C (2012) Some applications of Adaptive Neuro-Fuzzy Inference System (ANFIS) in geotechnical engineering. Comput Geotech 40:14–33

Chang C (2004) Empirical rock strength logging in boreholes penetrating sedimentary formations. Geophys Geophys Explor 7(3):174–183

Chang C, Zoback M, Khaksar A (2006) Empirical relations between rock strength and physical properties in sedimentary rocks. J Petrol Sci Eng 51(3–4):223–237
Chen X, Zhang R, Zhao X, Yang J, Lan Z, Luo C, Cai J (2023) Multifractal estimation of NMR T_2 cut-off value in low-permeability rocks considering spectrum kurtosis: SMOTE-based oversampling integrated with machine learning. Petrol Sci. https://doi.org/10.1016/j.petsci.2023.08.001
Dessouki M, Myers M, Hathon L (2016) The effect of CEC, salinity, mineralogy, and grain-size distribution on resedimented mudrock strength obtained through multistage triaxial testing. In: SEG international exposition and annual meeting, SEG-2016-13971461, Dallas
Dewhurst D, Sarout J, Piane C, Siggins A, Raven M (2015) Empirical strength prediction for preserved shales. Mar Petrol Geol 67:512–525
Escartín J, Andreani M, Hirth G, Evans B (2008) Relationships between the microstructural evolution and the rheology of talc at elevated pressures and temperatures. Earth Planet Sci Lett 268(3–4):463–475
Fakir M, Ferentinou M, Misra S (2017) An investigation into the rock properties influencing the strength in some granitoid rocks of KwaZulu-Natal, South Africa. Geotech Geol Eng 35:1119–1140
Farid H, Saeidi A, Farzaneh M (2017) Prediction of failure in atmospheric ice under triaxial compressive stress. Cold Reg Sci Technol 138:46–56
Farrokhrouz M, Asef M (2017) Experimental investigation for predicting compressive strength of sandstone. J Nat Gas Sci Eng 43:222–229
Forquin P, Arias A, Zaera R (2008) Role of porosity in controlling the mechanical and impact behaviours of cement-based materials. Int J Impact Eng 35(3):133–146
Forquin P, Safa K, Gary G (2010) Influence of free water on the quasi-static and dynamic strength of concrete in confined compression tests. Cement Concrete Res 40(2):321–333
Ge X, Fan Y, Zhu X, Chen Y, Li R (2015) Determination of nuclear magnetic resonance T_2 cutoff value based on multifractal theory—an application in sandstone with complex pore structure. Geophysics 80(1):D11–D21
Ge X, Xiao Y, Fan Y, Liu J, Zhang Y (2020) Laboratory investigation of the relationship between static rock elastic parameters and low field nuclear magnetic resonance data. Int J Rock Mech Min 127:104207
Ge X, Mao G, Hu S, Li J, Zuo F, Zhang R, Xing L (2023) Laboratory NMR study to quantify the water saturation of partially saturated porous rocks. Lithosphere 2023:1214083
Gharechelou S, Aminia A, Bohloli B, Swennen R (2020) Relationship between the sedimentary microfacies and geomechanical behavior of the Asmari Formation carbonates, southwestern Iran. Mar Petrol Geol 116:104306
Griffiths L, Heap M, Xu T, Chen C, Baud P (2017) The influence of pore geometry and orientation on the strength and stiffness of porous rock. J Struct Geol 96:149–160
Gullu H, Hazirbaba K (2010) Unconfined compressive strength and post-freeze-thaw behavior of fine-grained soils treated with geofiber and synthetic fluid. Cold Reg Sci Technol 62(2–3):142–150
Haimson B (2011) Consistent trends in the true triaxial strength and deformability of cores extracted from ICDP deep scientific holes on three continents. Tectonophysics 503(1–2):45–51
Hashiba K, Fukui K, Kataoka M (2019) Effects of water saturation on the strength and loading-rate dependence of andesite. Int J Rock Mech Min 117:142–149
Hassanvand M, Moradi S, Fattahi M, Zargar G, Kamari M (2018) Estimation of rock uniaxial compressive strength for an Iranian carbonate oil reservoir: modeling vs. artificial neural network application. Petrol Res 3(4):336–345
Heap MJ, Lavallée Y, Petrakova L, Baud P, Reuschlé T, Varley N, Dingwell D (2014) Microstructural controls on the physical and mechanical properties of edifice-forming andesites at Volcán de Colima, Mexico. J Geophys Res Sol Earth 119(4):2925–2963
Huang Y, Xiao J, Zhang C (2012) Theoretical study on mechanical behavior of steel confined recycled aggregate concrete. J Constr Steel Res 76:100–111
Kandiri A, Golafshani E, Behnood A (2020) Estimation of the compressive strength of concretes containing ground granulated blast furnace slag using hybridized multi-objective ANN and salp swarm algorithm. Constr Build Mater 248:118676
Kapang P, Walsri C, Sriapai T, Fuenkajorn K (2013) Shear strengths of sandstone fractures under true triaxial stresses. J Struct Geol 48:57–71
Khaksar A, Taylor PG, Fang Z, Kayes TJ, Salazar A, Rahman K (2009) Rock strength from core and logs, where we stand and ways to go. In: EUROPEC/EAGE conference and exhibition. SPE-121972-MS, Amsterdam
Kitamura M, Hirose T (2017) Strength determination of rocks by using indentation tests with a spherical indenter. J Struct Geol 98:1–11
Kumar RR, Rao DG (2012) Review of methods for uniaxial compressive rock strength estimation in deepwater formation with uncertainty quantification in wellbore stability analysis in absence of core measurements. In: SPE deepwater drilling and completions conference. SPE-150343-MS, Galveston
Li J, Zhu L, Zhou K, Cao S, Liu H (2019) Experimental investigation on the effects of ambient freeze-thaw cycling on creep mechanical properties of sandstone under step loading. IEEE Access 7:108513–108520
Lisabeth HP, Zhu W (2015) Effect of temperature and pore fluid on the strength of porous limestone. J Geophys Res Sol Earth 120(9):6191–6208
Liu Q, Huang S, Kang Y, Liu X (2015) A prediction model for uniaxial compressive strength of deteriorated rocks due to freeze-thaw. Cold Reg Sci Technol 120:96–107
Lou Y, Yoon JW, Huh H, Chao Q, Song J (2018) Correlation of the maximum shear stress with micro-mechanisms of ductile fracture for metals with high strength-to-weight ratio. Int J Mech Sci 146–147:583–601
Luo H, Cooper WL, Lu H (2014) Effects of particle size and moisture on the compressive behavior of dense Eglin sand under confinement at high strain rates. Int J Impact Eng 65:40–55
Maleki M, Bayat M (2012) Experimental evaluation of mechanical behavior of unsaturated silty sand

under constant water content condition. Eng Geol 141–142:45–56
Meng Z, Zhang J, Peng S (2006) Influence of sedimentary environments on mechanical properties of clastic rocks. Environ Geol 51:113–120
Nadah J, Bignonnet F, Davy C, Skoczylas F, Troadec D, Bakowski S (2013) Microstructure and poro-mechanical performance of Haubourdin chalk. Int J Rock Mech Min 58:149–165
Najibi AR, Ghafoori M, Lashkaripour G, Asef M (2015) Empirical relations between strength and static and dynamic elastic properties of Asmari and Sarvak limestones, two main oil reservoirs in Iran. J Petrol Sci Eng 126:78–82
Negara A, Ali S, Aldhamen A, Kesserwan H, Jin G (2017) Unconfined compressive strength prediction from petrophysical properties and elemental spectroscopy using support-vector regression. In: SPE Kingdom of Saudi Arabia technical symposium and exhibition, SPE-188077-MS, Dammam
Olea IV, Shirkavand F, Kustamsi A, Hareland G, Nygaard R, Hayes J, Teichrob R (2008) Correlation of sonic log values to strength in salt. In: The 42nd US rock mechanics symposium. ARMA-08-277, San Francisco
Onyia EC (1988) Relationships between formation strength, drilling strength, and electric log properties. In: SPE annual technical conference and exhibition. SPE-18166-MS, Houston
Pan J, Meng Z, Hou Q, Ju Y, Cao Y (2013) Coal strength and Young's modulus related to coal rank, compressional velocity and maceral composition. J Struct Geol 54:129–135
Peng J, Wong LNY, Teh CI (2017) Influence of grain size heterogeneity on strength and microcracking behavior of crystalline rocks. J Geophys Res Sol Earth 122(2):1054–1073
Rabah H, Yahia A, Boukhili R (2014) Triaxial compressive strength of concrete subjected to high temperatures. J Mater Civil Eng 26(4):705–712
Rabbani E, Sharif F, Salooki M, Moradzadeh A (2012) Application of neural network technique for prediction of uniaxial compressive strength using reservoir formation properties. Int J Rock Mech Min 56:100–111
Rafiai H, Jafari A (2011) Artificial neural networks as a basis for new generation of rock failure criteria. Int J Rock Mech Min 48(7):1153–1159
Rohmer J, Pluymakers A, Renard F (2016) Mechano-chemical interactions in sedimentary rocks in the context of CO_2 storage: weak acid, weak effects? Earth Sci Rev 157:86–110
Sharma M, O'Regan M, Baxter C, Moran K, Vaziri H, Narayanasamy R (2010) Empirical relationship between strength and geophysical properties for weakly cemented formations. J Petrol Sci Eng 72(1–2):134–142
Shen W, Shao J (2016) An elastic-plastic model for porous rocks with two populations of voids. Comput Geotech 76:194–200
Silva G, Rabe C, Nunes A, Garcia J, Prasad U (2015) Development of a new correlation based on grain size distribution to estimate sandstone reservoir uniaxial compressive strength. In: 13th ISRM international congress of rock mechanics. ISRM-13CONGRESS-2015-067, Montreal
Talesnick M, Hatzor Y, Tsesarsky M (2001) The elastic deformability and strength of a high porosity, anisotropic chalk. Int J Rock Mech Min 38(4):543–555
Tang S (2018) The effects of water on the strength of black sandstone in a brittle regime. Eng Geol 239:167–178
Testamanti M, Rezaee R (2017) Determination of NMR T_2 cut-off for clay bound water in shales: a case study of Carynginia Formation, Perth Basin, Western Australia. J Petrol Sci Eng 149:497–503
Tokle K, Horsrud P, Bratli R (1986) Predicting uniaxial compressive strength from log parameters. In: SPE annual technical conference and exhibition. SPE-15645-MS, New Orleans
Tsiambaos G, Sabatakakis N (2004) Considerations on strength of intact sedimentary rocks. Eng Geol 72(3–4):261–273
Ündül Ö (2016) Assessment of mineralogical and petrographic factors affecting petro-physical properties, strength and cracking processes of volcanic rocks. Eng Geol 201:10–22
Vapnik Y, Palchik V, Galuskina I, Banasik K, Krzykawski T (2018) Mineralogy, chemistry and rock mechanic parameters of katoite-bearing rock from the Hatrurim Basin, Israel. J Afr Earth Sci 147:322–330
Wang Z, Li W, Wang Q, Liu S, Hu Y, Fan K (2019) Relationships between the petrographic, physical and mechanical characteristics of sedimentary rocks in Jurassic weakly cemented strata. Environ Earth Sci 78:131
Wang S, Xu W, Yan L, Feng X, Xie W, Chen H (2020) Experimental investigation and failure mechanism analysis for dacite under true triaxial unloading conditions. Eng Geol 264:105407
Xiao L, Mao Z, Li G, Jin Y (2012) Calculation of porosity from nuclear magnetic resonance and conventional logs in gas-bearing reservoirs. Acta Geophys 60(4):1030–1042
Xiao L, Li J, Mao Z, Lu J, Yu H, Guo H, Li G (2018) A method to determine nuclear magnetic resonance (NMR) T_2cutoff based on normal distribution simulation in tight sandstone reservoirs. Fuel 225:472–482
Xu H, Tang D, Zhao J, Li S (2015) A precise measurement method for shale porosity with low-field nuclear magnetic resonance: a case study of the Carboniferous-Permian strata in the Linxing area, eastern Ordos Basin, China. Fuel 143:47–54
Xu H, Zhou W, Xie R, Da L, Xiao C, Shan Y, Zhang H (2016) Characterization of rock mechanical properties using lab tests and numerical interpretation model of well logs. Math Probl Eng 2016:5967159
Yagiz S (2009) Assessment of brittleness using rock strength and density with punch penetration test. Tunn Undergr Sp Technol 24(1):66–74
Yang S, Xu P, Li Y, Huang Y (2017) Experimental investigation on triaxial mechanical and permeability behavior of sandstone after exposure to different high temperature treatments. Geothermics 69:93–109
Yang X, Weng L, Hu Z (2018) Damage evolution of rocks under triaxial compressions: an NMR investigation. KSCE J Civ Eng 22(8):2856–2863
Yang S, Yin P, Huang Y, Cheng J (2019) Strength, deformability and X-ray micro-CT observations of transversely isotropic composite rock under different confining pressures. Eng Fract Mech 214:1–20

Yin P, Yang S (2018) Experimental investigation of the strength and failure behavior of layered sandstone under uniaxial compression and Brazilian testing. Acta Geophys 66:585–605

Zhai C, Wu S, Liu S, Qin L, Xu J (2017) Experimental study on coal pore structure deterioration under freeze–thaw cycles. Carpath J Earth Env 76:507

Zhao Y, Wan Z, Feng Z, Yang D, Zhang Y, Qu F (2012) Triaxial compression system for rock testing under high temperature and high pressure. Int J Rock Mech Min 52:132–138

Zhong S, Baitalow F, Nikrityuk P, Gutte H, Meyer B (2014) The effect of particle size on the strength parameters of German brown coal and its chars. Fuel 125:200–205

Zingg L, Briffaut M, Baroth J, Malecot Y (2016) Influence of cement matrix porosity on the triaxial behaviour of concrete. Cement Concrete Res 80:52–59